Laboratory observations of wave evolution, modulation and blocking due to spatially varying opposing currents

Y. MA[1]†, G. DONG[1], M. PERLIN[2], X. MA[1], G. WANG[1] AND J. XU[3]

[1]State Key Laboratory of Coastal and Offshore Engineering, Dalian University of Technology, Dalian 116023, China

[2]Department of Naval Architecture and Marine Engineering, University of Michigan, Ann Arbor, MI 48109, USA

[3]CCCC-Fourth Harbor Design Institute Engineering Company Ltd., Guangzhou 510230, China

The nonlinear evolution of waves propagating on a spatially varying opposing current has been observed in a wave–current flume. Regular waves with different initial periods and different initial steepness, s $(0.05 < s < 0.19)$, were generated and observed. Frequency downshift, even with very small initial steepness, was identified. As expected, it was found that opposing currents can have significant interactions with wavetrains. The ultimate frequency downshift increases with the increase in initial steepness. The evolution of frequency modulation was observed via the instantaneous frequency extracted by the Morlet-wavelet transform. The instantaneous frequency showed that often the process of frequency downshift can be local in time and gradual, but abrupt changes of local frequency were also detected. The presence of an opposing current can gradually block the primary wave energy and destroy the conservation of the wave action at downwave locations, thus increasing the asymmetric modulation and accelerating the effective frequency downshift.

Key words: surface gravity waves, wave breaking

1. Introduction

An important problem of surface waves propagating into regions of decreasing depth that remains largely unsolved is that of waves travelling against an opposing current. This problem is fundamental to several physically relevant situations for coastal and ocean engineering as well as of interest to those who study general wave phenomena. Many interesting observations arise as a consequence of this interaction between waves and currents including gradual and abrupt frequency downshift and complete blockage of the waves. This paper discusses these processes as established through a laboratory investigation.

To begin, a brief discussion of wave–wave interaction, of which wave–current interaction can be considered as a special case, is appropriate, and in particular the associated frequency-downshift phenomenon is relevant here. One kind of wave–wave

† Email address for correspondence: yuxma@126.com

interaction is the so-called 'resonant' interaction, which for gravity waves generally involves four or more wave components and may require many wavelengths/periods to transfer energy among free waves; resonant interactions are dominant mainly in deep and intermediate water (Phillips 1960; Hasselmann 1962). Nonlinear resonant wave–wave interactions in deep and intermediate depth can lead to wave modulation of both amplitude and frequency. Wave modulations are very important in ocean engineering and can have important consequences for marine structures. One obvious result caused by nonlinear resonant interactions is the frequency downshift (the wave peak-frequency shift from the initial dominant frequency to a lower one) which is closely related to the Benjamin–Feir sideband instability, a degenerate four-wave resonant interaction (Benjamin & Feir 1967). Due to the existence of the frequency downshift, waves can be more stable and have the potential to grow higher and propagate faster (Huang, Long & Shen 1996).

Over the past several decades, much effort has been expended to determine the mechanisms of modulation of deep-water waves, and many insightful results have been obtained from both numerical and experimental approaches. Significant progress has been made to explain the physical mechanisms of the frequency-downshift phenomenon. Lake *et al.* (1977) first observed the frequency-downshift phenomenon in experiments by observing the long-time evolution of deep-water waves. Later, Melville (1982) and Su (1982) also found the frequency downshift in their experiments. They suggested that the phenomenon was closely related to the Benjamin–Feir instability, and occurred following wave breaking. However, no plausible physical mechanism of the frequency downshift was given by either Melville (1982) or Su (1982). Ramamonjiarisoa & Mollo-Christensen (1979) used 'crest pairing' (which is a phenomenon where one crest overtakes the previous crest and disappears, resulting in a local increase of period) to explain the abnormal phenomenon. Chereskin & Mollo-Christensen (1985) also suggested that crest pairing is the mechanism responsible for the frequency downshift and that the process was gradual. Melville (1983) analysed the process of deep-water wave modulation in detail, and used phase reversals to explain the frequency downshift that appeared after wave breaking. Huang *et al.* (1996) gave a detailed analysis of deep-water wave modulation. Their explanation of the mechanism of frequency downshift was a 'wave fusion' process, and they suggested that the process was local, discrete and abrupt. Experiments on the evolution of wave modulation with known initial sidebands (the upper and lower frequency sidebands were simultaneously imposed by the signal sent to the wave generator) were also conducted (Tulin & Waseda 1999; Chiang & Hwung 2007; Hwung, Chiang & Hsiao 2007); temporary frequency downshift was observed in non-breaking cases, which is consistent with the theoretical result of Lo & Mei (1985), but permanent frequency downshift occurred only after breaking. Wind effects on nonlinear wave modulation were also considered by both numerical (Hara & Mei 1991) and experimental (Waseda & Tulin 1999) methods.

In estuary regions, currents are usually strong and hence their influence on waves cannot be ignored. As waves propagate onto an opposing current, their group velocity is reduced and significant energy transfer among wave components can occur in a very short distance. If an opposing current is sufficiently strong, then the wave group velocity, C_g, can go to zero, causing the waves to become blocked (Chawla & Kirby 2002). Chawla & Kirby (2002) found that the frequency downshift occurs with opposing currents present, even in the absence of breaking, indicating that an opposing current can play an important role in the process of frequency downshift.

Turpin, Benmoussa & Mei (1983) derived a cubic nonlinear Schrödinger equation that included the effects of currents and varying depth. The numerical results showed that the instability parameter is a function of variation of currents and depth. A following current has a stabilizing effect on a wavetrain, but an opposing current can cause major wavetrain changes in all depths. Gerber (1987) studied the influence of non-uniform currents on the Benjamin–Feir instability of deep-water waves using another nonlinear Schrödinger equation. Gerber (1987) also showed that following currents have a stabilizing effect on the waves while an opposing current can cause a rapid instability. He explained that following currents reduce wave steepness and therefore a longer time is required than in quiescent water for the same growth of the sidebands. As an opposing current has a steepening effect on waves, it can shorten the required time for the growth of the sidebands. Recently, van Duin (1999) considered current non-uniformity on the development of modulated wavepackets, and found similar results to Turpin *et al.* (1983) and Gerber (1987). Compared with theoretical and numerical studies, laboratory observation of the modulation of waves in currents has lagged behind. Even though the frequency-downshift phenomenon was observed in previous experimental studies on wave–current interactions (Lai, Long & Huang 1989; Chawla & Kirby 2002), the details of wave modulation on opposing currents are still unresolved. For example, how do waves evolve in currents? Are there any differences between breaking and non-breaking cases? Is the physical mechanism of the frequency downshift in a current the same as in quiescent water? Is the characteristic of the frequency downshift gradual or abrupt? Aside from steepening waves and more rapid energy transfer, are there other influences of opposing currents on waves? To address the above issues, experiments were carried out in a wave–current flume. Regular waves with different initial periods and different steepness ($0.05 < s < 0.19$, where s is defined as ka with k being the wavenumber and a being the wave amplitude at the first measure location) propagating in opposing currents with spatial variation along the flume were considered.

This paper is organized as follows. In §2, the experimental instrumentation and measurement techniques are discussed. In §3, the analytical methods used in this study are presented. A discussion of the detailed analysis and results of the measured wave modulation is presented in §4. Lastly, the conclusions of this research are given in §5.

2. Experimental set-up

2.1. *Wave flume*

The experiments were conducted in the wave flume at the State Key Laboratory of Coastal and Offshore Engineering, Dalian University of Technology, Dalian, China. This flume is 50.0 m long, 3.0 m wide and was used with a water depth of 0.5 m. The detailed experimental set-up is shown in figure 1. The tank is equipped with a hydraulically driven piston-type wavemaker and in the following $x = 0$ m is defined as the mean position of the wavemaker. For this depth, currents to 0.26 m s^{-1} can be generated by a pump located near the wavemaker end of the flume. The pipe system allows the flow of water in either direction. In this paper, only adverse currents were generated. As can be seen in figure 1, to facilitate the current flow and weaken the effect of any inflow vortices on wave generation, two four-layer wire mesh screens with hole size of 55 mm and a wire diameter of 1 mm were placed at the current inlet and at the outlet. To create a gradient in the current field, a smooth impermeable submerged bar, 0.25 m in height and 6.0 m in length along its constant-depth portion,
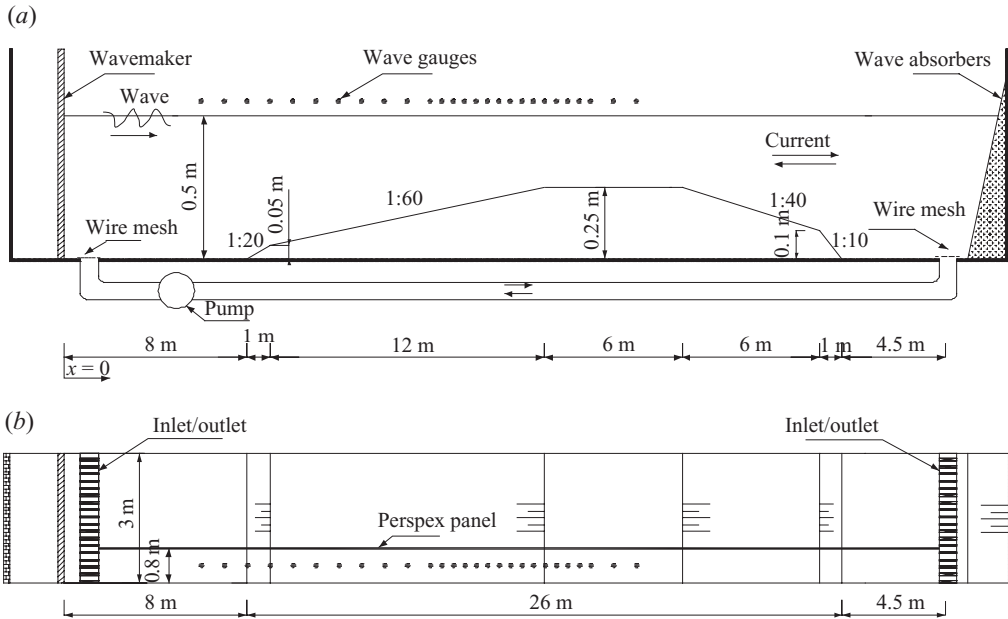
(*a*)

(*b*)

FIGURE 1. Schematic view of the experimental set-up. (*a*) Elevation view. (*b*) Plan view.

was installed near the middle of the flume. Therefore, along the horizontal portion of the bar, the water depth was reduced to 0.25 m. The seaward slope of the bar was 1:60 with a 1 m long approach slope (1:20); the rearward slope of the bar was 1:40 with a 1 m long exit slope (1:10). The flume was subdivided longitudinally into two sections with widths of 0.8 and 2.2 m by a Perspex wall, starting from $x = 1.5$ m and continuing downwave to the end of the tank. The narrower 0.8 m wide section was chosen as the working section to ensure two-dimensionality of the wave field (i.e. to suppress the three-dimensional instability observed by Su 1982). Owing to the low friction of glass and Perspex, the influence of the sidewalls on the flow was relatively small.

The water-surface elevations were recorded with 27 capacitance wave gauges, which are delineated by filled circles in figure 1. These gauges were placed with a relatively coarse spacing of 1.0 m in deeper water, which was reduced to 0.5 m from the middle part of the seaward slope of the bar to the middle of the top of the bar. The absolute accuracy of these wave gauges was of the order of ± 1 mm. Before the wave gauges were used, they were re-calibrated to ensure their accuracy during the experiments. The duration of each record was 102.4 s; relatively short series were necessitated to avoid reflection by the end of the flume. The sampling frequency was 40 Hz.

Current measurements were made using a Nortek acoustic Doppler velocimeter (ADV, velocity range 1 m s^{-1}, sampling rate 200 Hz) with a specified accuracy of 1 mm s^{-1}. Detailed measurements of the vertical current profile along the centreline of the working section of the flume were conducted. Each measurement of current was conducted following 40 min of flow to let the unsteadiness decay. These measurements were repeated three times for each test run, and along with the measured wave parameters, H, T and the frequency downshift were within the instrumentation-specified error, indicating that the experiments were repeatable. Figure 2 shows the mean current (averaged over 240 s) profile at five different locations along the flume.
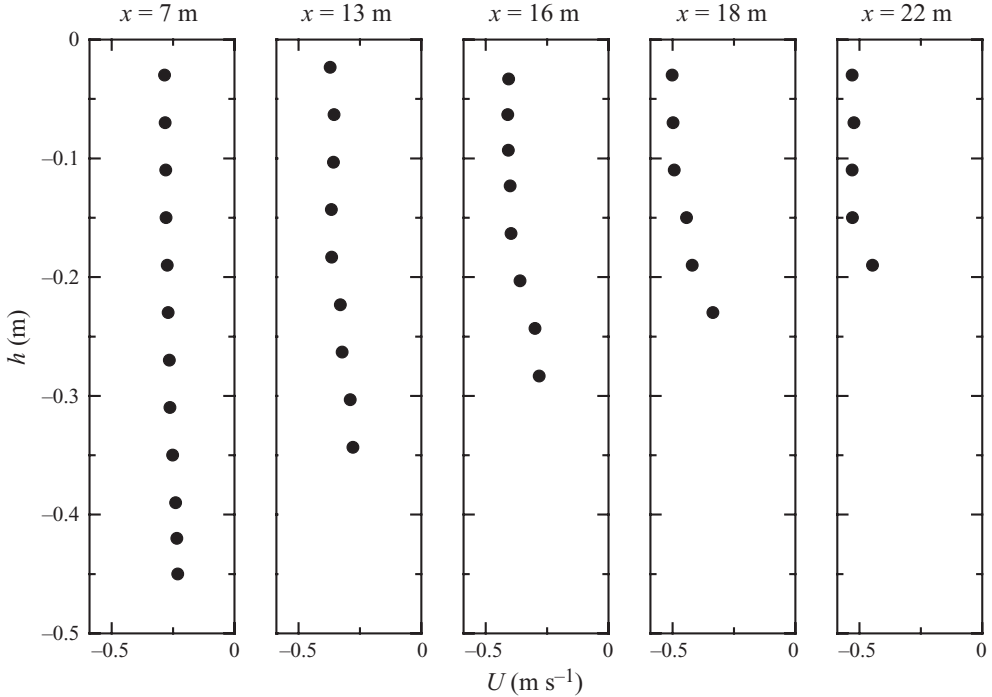
FIGURE 2. Vertical mean current profile at five different locations in the flume. Note that the missing points downwave are due to bottom profile changes.

In the absence of waves, these current profiles followed the expected boundary-layer shape, especially the closer they were measured to the source. Essentially uniform current profiles were found from the surface to at least 20 cm below the surface. Hence, the variations of current over depth are ignored. In the absence of waves, the mean current along the flume is shown in figure 3, which reflects the changes of cross-sectional area very well using the conservation of volume flux. As a result of the change in water depth, the depth-averaged current varied from $0.255\,\mathrm{m\,s^{-1}}$ at $x = 7\,\mathrm{m}$ to its maximum value of $0.520\,\mathrm{m\,s^{-1}}$ at $x = 22\,\mathrm{m}$. The same current conditions were implemented for all the experiments.

2.2. *Wave conditions*

A total of 12 experiments with regular waves of different periods, T, and steepness, s, were considered. Details of the tests are presented in table 1. The wave-number k was estimated using the Doppler-shift linear dispersion relation for waves on a constant depth (i.e. $(\omega - Uk)^2 = gk\tanh(kh)$, where g is the gravity due to acceleration, U is the current and ω is the radian frequency) at $x = 6\,\mathrm{m}$. The height H was the mean height of the waves recorded at $x = 6\,\mathrm{m}$, and it was used to determine the initial steepness, s, of each case. The relative water depth kh at $x = 6\,\mathrm{m}$ ranges from 1.4 to 3.3, and in the vicinity of the bar, even though the water depth is less, the values of kh can be higher due to the presence of the stronger opposing current. Hence, the waves generated in the experiments can be classified as propagating in intermediate water depth.

Case	T (s)	H (cm)	kh	s or ka
1	1.0	2.21	3.3	0.073
2	1.0	3.2	3.3	0.106
3	1.0	5.54	3.3	0.183
4	1.1	2.5	2.6	0.065
5	1.1	3.37	2.6	0.087
6	1.1	5.7	2.6	0.148
7	1.2	2.61	2.12	0.055
8	1.2	5.23	2.12	0.11
9	1.2	6.76	2.12	0.14
10	1.5	3.3	1.39	0.046
11	1.5	5.75	1.39	0.08
12	1.5	8.29	1.39	0.115

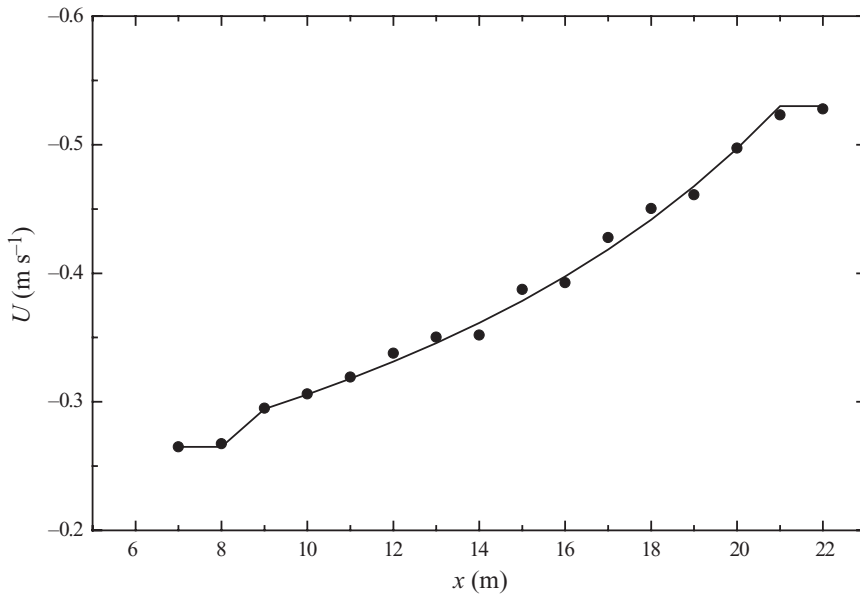TABLE 1. Wave conditions at $x = 6$ m.

FIGURE 3. Averaged current U as a function of x (with no wave generation). Filled circles represent the measured data; the curve represents the flow using the conservation of volume flux.

3. Analytical method

3.1. *Wave spectra*

Wave spectra can provide the energy distribution as a function of frequency. From the spectrum, the evolution of the peak frequency f_p and variations of the sideband energy can be detected. In this study, wave spectra were obtained by fast Fourier transform (FFT), and then the spectra were smoothed by a 10-point running average; thus each spectral estimate has 20 degrees of freedom.

3.2. *Instantaneous peak-frequency content*

A traditional method to calculate the instantaneous frequency content of a signal is through the Hilbert transform. As a different procedure is usually adopted to

calculate the instantaneous frequency, some incorrect frequencies, such as a negative frequency, will be obtained by using the Hilbert transform of a composite signal. Delprat *et al.* (1992) showed that the ridges of the continuous wavelet transform of a signal can represent the instantaneous frequencies of that signal. The instantaneous frequencies extracted from the wavelet transforms can detect the rapid changes of frequency (Mallat 1999). In this study the instantaneous peak frequencies of the measured waves were obtained from the ridge of a Morlet-wavelet transform (Kijewski-Correa & Kareem 2006). In general, the continuous wavelet transform of an arbitrary time series $\xi(t)$ can be obtained by dilating in scale a, which is inversely proportional to frequency, and translating in τ the mother wavelet $\psi(t)$:

$$WT(a, \tau) = \frac{1}{\sqrt{a}} \int_{-\infty}^{\infty} \xi(\tau) \psi^* \left(\frac{t - \tau}{a} \right) \mathrm{d}\tau, \tag{3.1}$$

where the asterisk denotes the complex conjugate. To seek the harmonic character of signals, the Morlet wavelet is often adopted:

$$\psi(t') = \pi^{-1/4} \exp\left(-\frac{t'^2}{2} \right) \exp(\mathrm{i}\omega_c t'). \tag{3.2}$$

The function of (3.2) is defined at unit scale. Here, ω_c is the central frequency of the wavelet and a parameter that determines the wavelet resolution (i.e. it relates the scale, a, to the Fourier frequencies). It should be larger than 6.0 to satisfy the admissibility condition (Farge 1992). A larger ω_c gives a finer frequency resolution at the expense of a poorer time resolution. In this study, ω_c was set to 12 to provide enhanced frequency resolution. Once a mother wavelet is chosen, it is necessary to choose a set of scales a to use in the wavelet transform. Conveniently, the scales can be written as fractional powers of two (Torrence & Compo 1998):

$$a_j = a_0 2^{j\delta}, \quad j = 0, 1, \dots, M, \tag{3.3}$$

$$M = \delta^{-1} \log_2 \left(\frac{N \Delta t}{a_0} \right), \tag{3.4}$$

where a_0 is the smallest scale and should be set to $2\Delta t$, Δt is the time interval, M is the number of scales, and N is the number of values in the time series. The parameter δ is the scale factor. The value of δ should be smaller than 0.5. Dilating the mother wavelet by the chosen scales, the wavelet transform defined in (3.1) can be completed. For the Morlet wavelet, the relationship between scale, a, and frequency, f, is defined (Torrence & Compo 1998) as

$$a = \frac{\omega_c + \sqrt{\omega_c^2 + 2}}{4\pi f}. \tag{3.5}$$

The wavelet energy spectrum can be defined as

$$P(a, \tau) = \frac{|WT(a, \tau)|^2}{a}. \tag{3.6}$$

The scale (frequency) having the maximum energy at each τ is the instantaneous peak frequency. Figure 4 illustrates the Morlet wavelet spectrum and the instantaneous peak frequencies for $x = 6\,\mathrm{m}$ of case 3. Based on the instantaneous peak frequencies extracted via the Morlet-wavelet transform of the measured wave series, the evolution of frequency modulation can be studied.
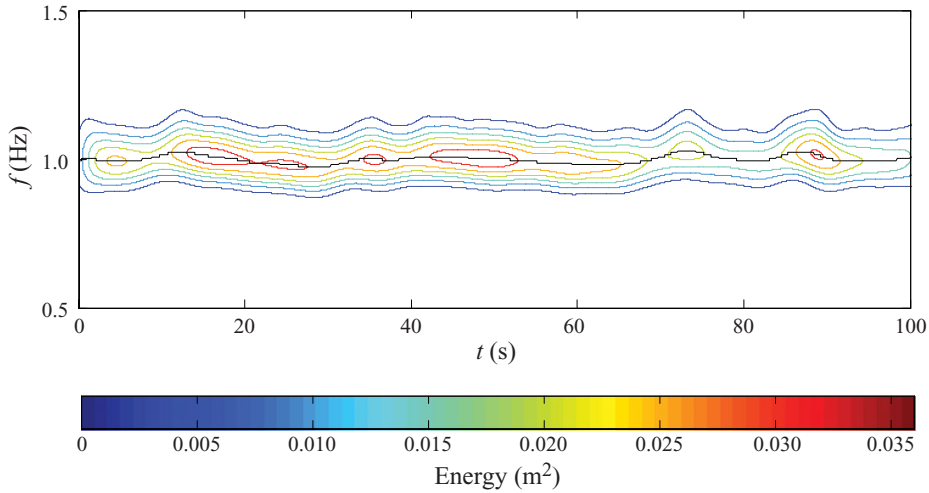
FIGURE 4. (Colour online) The wavelet spectrum contour for the surface elevations at $x = 6$ m for case 3. The black line represents the instantaneous peak frequencies of the wavetrain.

3.3. *Phase function*

A comparison of the phase functions is used to detect the local phase changes of time series. Here, the detrended phase function obtained by the Hilbert transform (Huang *et al.* 1992) was used to quantify the local phase changes of the wavetrains.

4. Results and discussion

4.1. *Peak frequency variations along the flume*

Figure 5 shows the variations of the non-dimensionalized peak frequency f_p (which were obtained by FFT) along the flume. For each experimental case, f_p at each location was non-dimensionalized by the peak frequency at $x = 6$ m. Frequency downshift is observed for cases 1–9 but not for cases 10–12. As mentioned previously, the current velocity on the top of the bar is 0.52 m s^{-1}. Based on the linear Doppler dispersion relation, free waves with frequency larger than 0.72 Hz should be blocked. Thus, the primary waves (including the carrier wave and the disturbed upper and lower sideband frequencies) for cases 1–9 should be blocked before waves reach the top of the bar as per linear theory. However, owing to the frequency downshift (for gravity waves lower frequency waves have larger phase speed and group velocity) and finite-amplitude dispersion, the blocking points of some experimental cases (cases 1, 2, 4 and 5) moved downwave, and for some cases (cases 3, 6–9), the wave blocking does not occur at all. Furthermore, for the blocked cases, the actual blocking locations are not consistent with the results calculated using the linear dispersion relation. For example, the peak frequency for case 1 is 0.91 Hz before blocking; hence, it should be blocked at $x = 17.5$ m based on the linear Doppler dispersion relation, but the actual blocking point is $x = 19.5$ m. Even for the non-blocked cases, primary waves should also be blocked at the horizontal portion of the bar based on the linear theory.

The third-order Stokes dispersion relation can be written as (Chawla & Kirby 2002):

$$(\omega - kU)^2 = gk \tanh kh \left[1 + (ka)^2 \left(\frac{8 + \cosh 4kh - 2 \tanh^2 kh}{8 \sinh^4 kh} \right) \right]. \qquad (4.1)$$
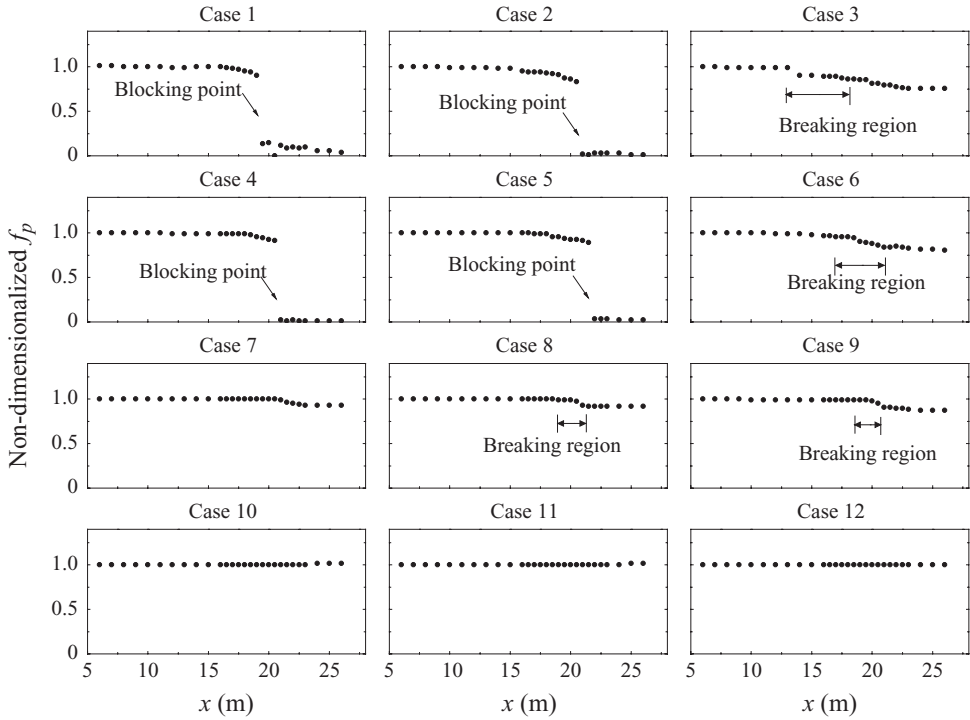
FIGURE 5. Variation of peak frequencies f_p, which were extracted from the spectra obtained by FFT, along the flume. For breaking cases, the breaking regions are marked in the corresponding panels. (For each case, f_p was non-dimensionalized by f_p measured at $x = 6$ m.)

The blocking points predicted by (4.1) are quite consistent with the actual blocking points for the blocked experimental cases (cases 1, 2, 4 and 5). Based on the third-order Stokes dispersion relation, cases 3, 6–9 cannot be blocked at the crest of the bar. This phenomenon indicates that the actual blocking criterion cannot be predicted by the linear dispersion relation, suggesting that numerical models, such as ones that use the wave-action equation (Bretherton & Garrett 1968), should use the third-order Stokes dispersion relation to predict wave dynamics close to the blocking point.

Furthermore, it should be noted that, in the presence of a blocking current, the frequency downshift can appear in non-breaking waves, which is consistent with the experiments of Chawla & Kirby (2002) over a constant depth. Cases with larger initial steepness exhibit larger frequency downshift (see table 2 and figure 6) that is approximately linear. It should be noted that the frequency downshift for the blocked cases (cases 1, 2, 4 and 5) was permanent as the primary waves (carrier, lower and upper sideband frequency waves) were blocked. For the other cases, some primary wave energy was blocked by the opposing current and the wave action was no longer conserved at the downwave stations. Due to the length limitation of the present tank, it is still questionable whether the frequency downshift is permanent. Experiments with different s in both quiescent water and a weaker opposing current, $U = 0.12 \, \text{cm s}^{-1}$ for horizontal depth $h = 0.5$ m, were also conducted but are not presented. No obvious modulation or frequency downshift was observed in those experiments, even for non-breaking experiments with initial s to 0.15.

Case	s or ka	Frequency downshift (%)
1	0.073	9
2	0.106	16
3	0.183	25
4	0.065	9
5	0.087	11
6	0.148	16
7	0.055	4
8	0.11	8
9	0.14	11
10	0.046	0
11	0.08	0
12	0.115	0

TABLE 2. Frequency downshift for the experimental cases.
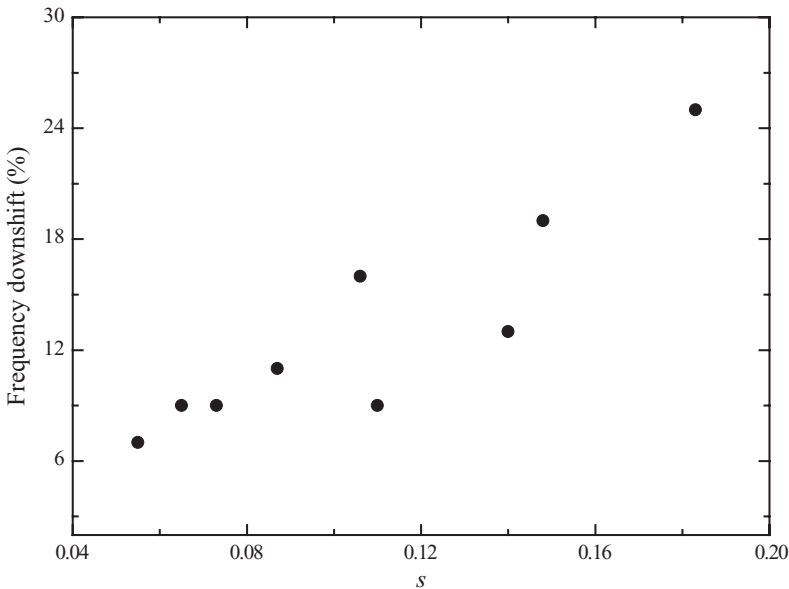
FIGURE 6. Variations of frequency downshift versus initial wave steepness.

4.2. *Modulation evolution of non-breaking waves*

The measured surface elevations of case 1 are shown in figure 7. The data recorded in the initial seconds at the locations beyond $x = 16.5\,\text{m}$ show little variation because the waves have not yet reached those locations. At the closest measured location ($x = 6\,\text{m}$), the waves already exhibited slight amplitude modulation. As the waves propagated and evolved, the amplitude modulations grew. At $x = 19.5\,\text{m}$, almost all the primary and sideband waves were blocked by the current. To examine the variations of the wave amplitude in the frequency domain, the amplitude spectra obtained by FFT at selected locations are shown in figure 8. At $x = 6\,\text{m}$, there was some low energy at the sidebands due to the background noise, such as $f_l = 0.94\,\text{Hz}$ and $f_u = 1.06\,\text{Hz}$. (Here, the subscripts l and u indicate lower and upper, respectively.) As the waves evolved, energy of the sidebands increased, as did the spectral width. It is evident that
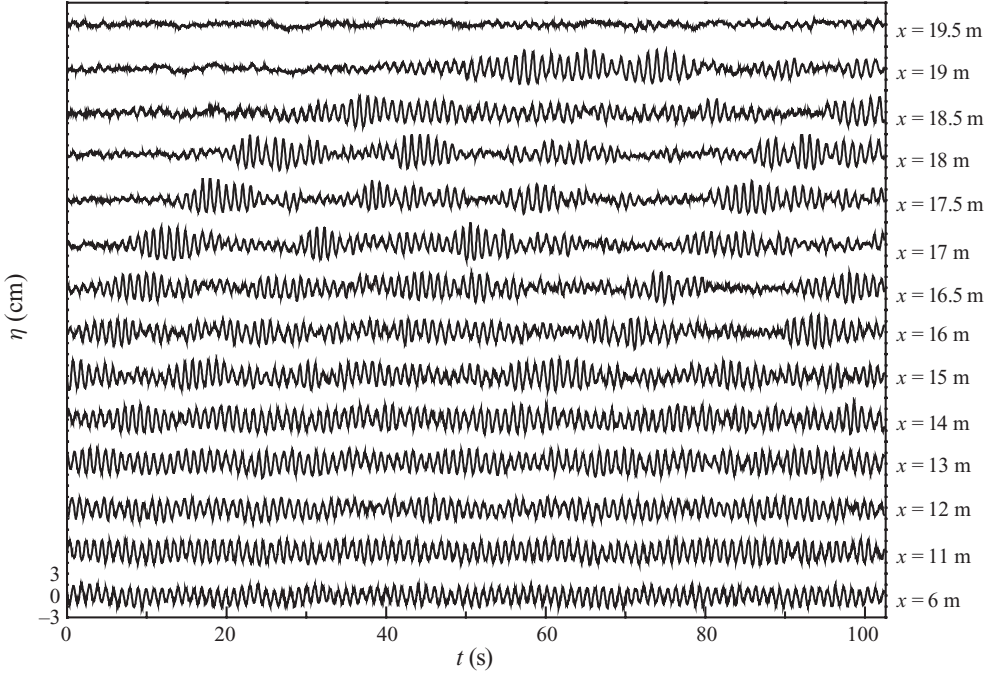
FIGURE 7. The measured surface elevations in the flume with an initial period 1.0 s and initial steepness 0.073 (non-breaking, case 1). Notice the increasing modulation of the wave envelope as the waves evolved. Also note that due to a reflection-issue limit, the initial parts of the wave records for $x > 16.5$ m show little change.

the evolution of the sidebands was not symmetric (i.e. the lower sideband grew with increasing distance, but the higher sideband exhibited little change). At $x = 17.5$ m, the energy of the lower lobe of the sideband was nearly equal to that of the initial wave peak frequency f_0. Eventually, the energy at the lower sideband overtook the energy of f_0 (at $x = 18$ m), and f_p became 0.94 Hz. Note that none of this occurred in the experiments conducted in both quiescent water and a weaker opposing current, even for waves with steepness s (at $x = 6$ m) twice as large as in this experimental case. Reiterating, the peak frequency of the waves moved to a lower frequency as the waves entered shallower water where an increased opposing current existed. With the increased strength of the opposing current, energy at the higher lobe of the sideband and its higher harmonics were gradually blocked. Furthermore, the widening of the spectrum suggests that the instability of the waves was not confined to several discrete frequencies, but was across a continuous frequency band, which is consistent with the results of Melville (1982) for deep-water conditions.

   In figure 8, the critical-blocking frequencies, which are predicted by both the linear and the third-order Stokes dispersion relation, are also identified. Free waves beyond these critical frequencies should be blocked by the local current. For the results predicted by the linear theory, it is noticed that there are significant primary waves that are not blocked by the local current, indicating that the blocking criterion as determined by the linear dispersion relation is not valid. Meanwhile, the third-order Stokes dispersion relation gives reasonable results, which is consistent with the work of Chawla & Kirby (2002). Notice that the local mean wave heights are adopted to calculate the third-order Stokes dispersion relation.
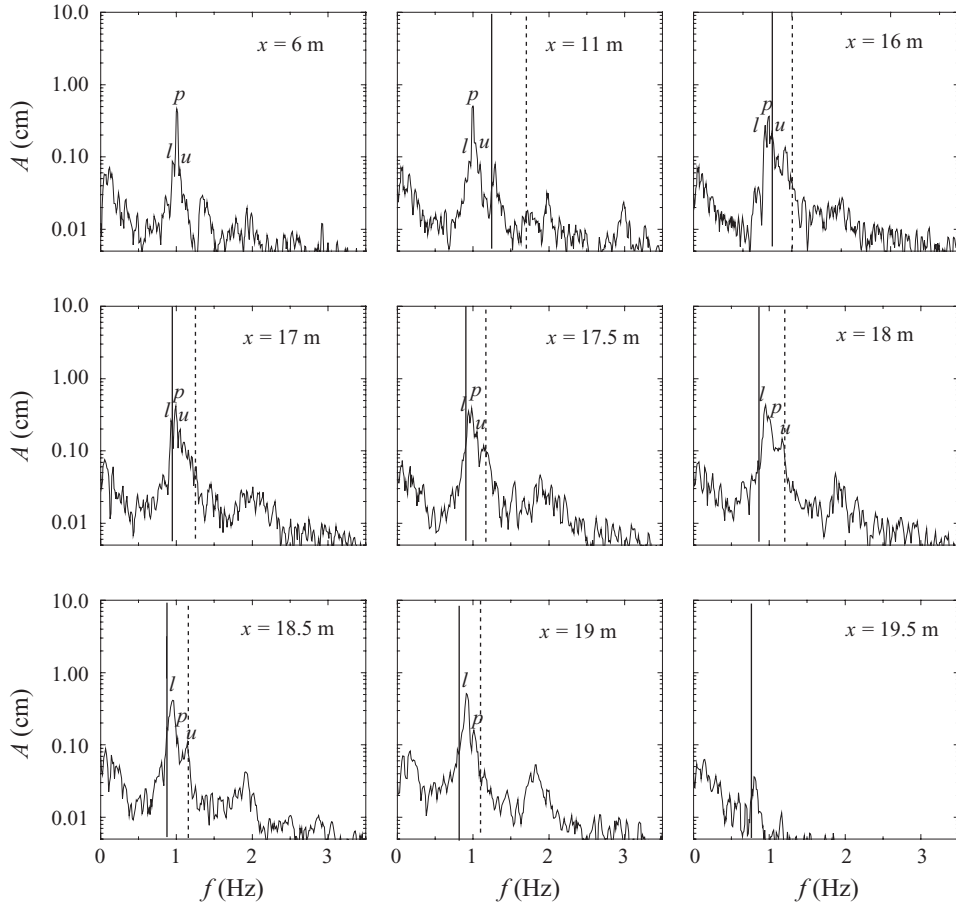
FIGURE 8. Evolution of spectra as a function of distance from the wavemaker for case 1 with initial $f_p = 1.0\,\mathrm{Hz}$ ('l' denotes the lower sideband, 'p' indicates the initial peak waves, 'u' denotes the upper sideband). Each spectral estimate has 20 degrees of freedom and is within $-23.5\,\%$ to $44.6\,\%$ of the 'true spectrum' at the 95 % confidence level. In these spectra, due to the recorded length changes, the frequency resolution is 0.01 Hz for $x < 17\,\mathrm{m}$, and for $x = 17\,\mathrm{m}$, $x = 17.5\,\mathrm{m}$, $x = 18\,\mathrm{m}$, $x = 18.5\,\mathrm{m}$, $x = 19\,\mathrm{m}$ and $x = 19.5\,\mathrm{m}$ the frequency resolution is 0.0105, 0.0112, 0.012, 0.013, 0.0142 and 0.015 Hz, respectively. The vertical solid lines in each graph identify the local critical frequencies based on the linear dispersion relation. The vertical dashed lines in each graph identify the local critical frequencies based on the third-order Stokes dispersion relation.

The above analysis provides the global variation of frequency, but it does not produce the frequency modulations of the waves. To examine the detailed frequency modulations, the variation of the instantaneous peak frequencies of waves extracted via the Morlet-wavelet transform are shown in figure 9. For convenient comparison, the corresponding wave elevations are shown simultaneously. At the closest measured location, even the instantaneous frequency was nearly uniform in time, and coincides with the initial f_p. The frequency modulation grew with distance and the time instantaneous frequencies were less than the initial f_p and gradually increased with increased distance downwave, indicating that the process of frequency downshift was gradual (see figure 9). At $x = 15\,\mathrm{m}$, there was local relatively large frequency downshift at times around 23 and 70 s, where wave amplitudes were small. As waves approached the top of the bar, abrupt changes of local peak frequency were observed, while the
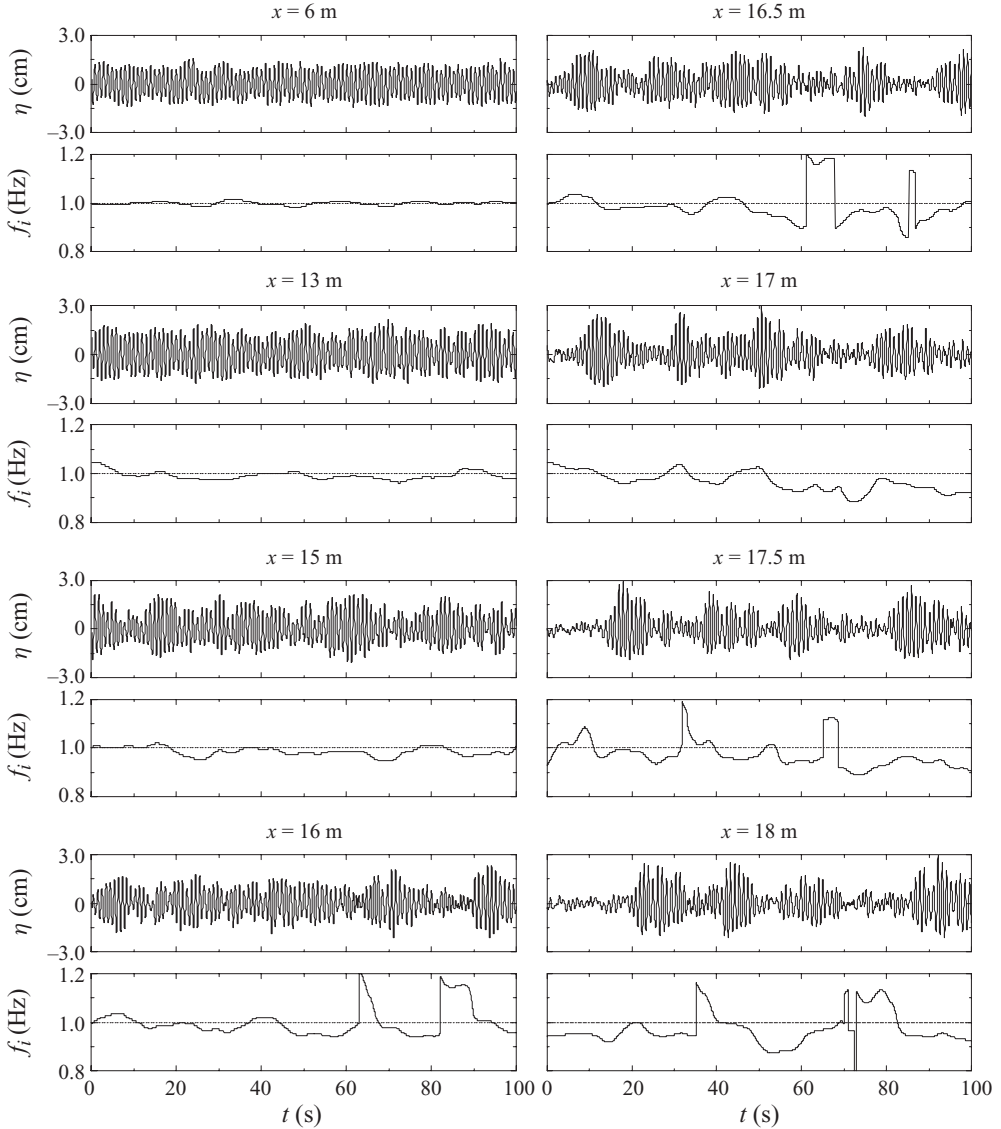
FIGURE 9. The evolution of the instantaneous peak frequency for case 1. The dotted line is the initial wave frequency. The instantaneous peak frequency was obtained by the Morlet-wavelet transform. The corresponding wave elevations are also shown for comparison.

amplitudes which correspond to those frequency changes were close to zero. There were not only abrupt peak frequency changes from lower to higher, but also from higher to lower. Even though abrupt local changes of peak frequencies existed, the global peak frequency gradually decreased to the lower sideband (see figure 5). It is interesting to see that those higher peak frequencies, which existed at the previous locations, do not exist at further downwave locations. For example, those larger peak frequencies which appeared suddenly at $x = 16$ m and $x = 16.5$ m (times around 65 and 85 s, respectively) vanished at $x = 17$ m. Those waves with higher frequency might be blocked by the current. To some extent, the existence of the opposing current can accelerate the process of frequency downshift. The mean values of the instantaneous peak frequencies for each measurement location shown in figure 9 and
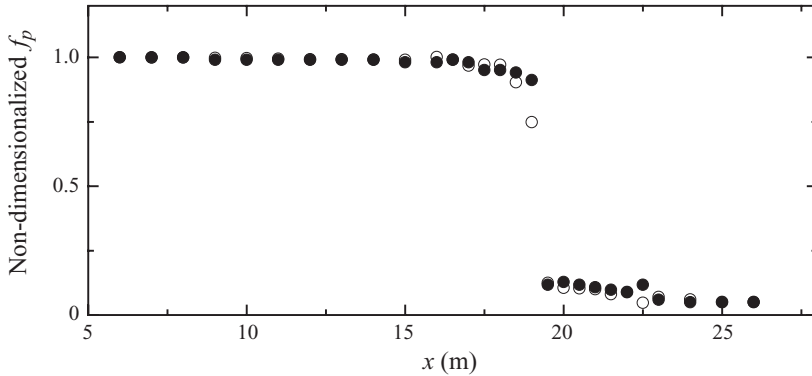
FIGURE 10. The mean values of the instantaneous peak frequencies (open circles) for case 1, non-dimensionalized by the result measured at $x = 6\,\text{m}$ along the flume. These data are the averages from figure 9 and other similar results that were not presented. The non-dimensionalized f_p (filled circles) obtained by FFT are also presented for comparison.
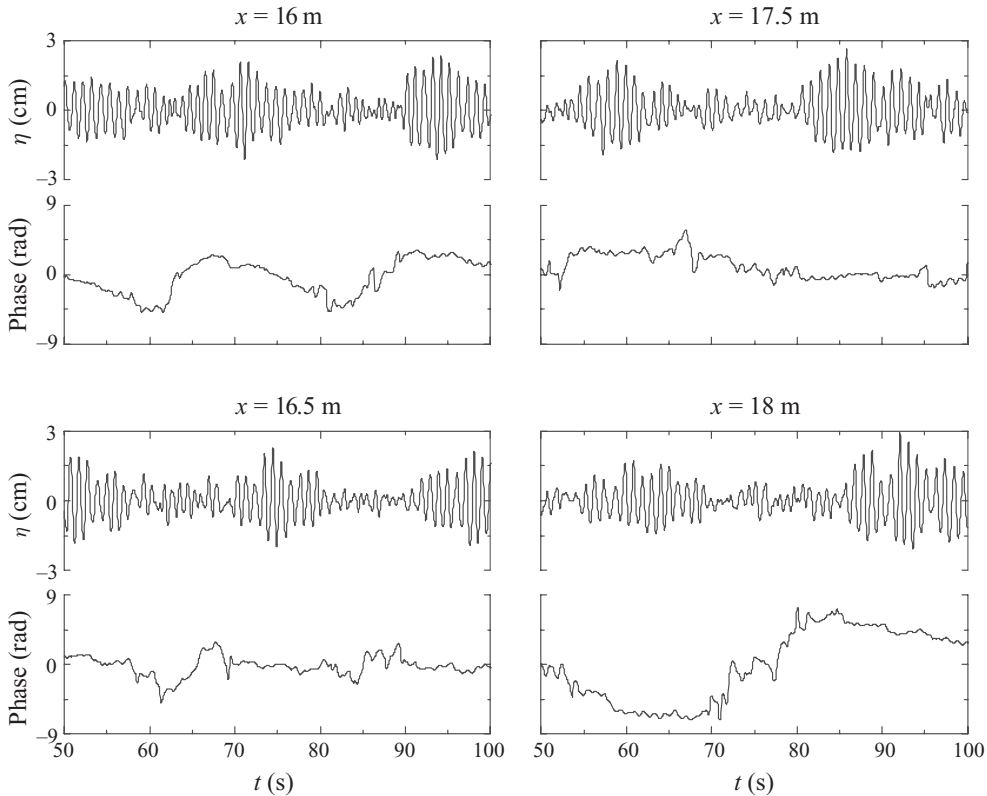

FIGURE 11. The detrended phase function of the surface elevations measured at four different locations for case 1.

some not presented are shown in figure 10. The mean values agree well with the results obtained via FFT, indicating that the method used to extract instantaneous frequency is meaningful and reasonable.

Figure 11 shows the detrended phase functions of the measured waves. As expected, at the time when the abrupt peak-frequency change occurs, there are local abrupt changes of phase. Thus, the abrupt peak frequency and phase changes correspond to
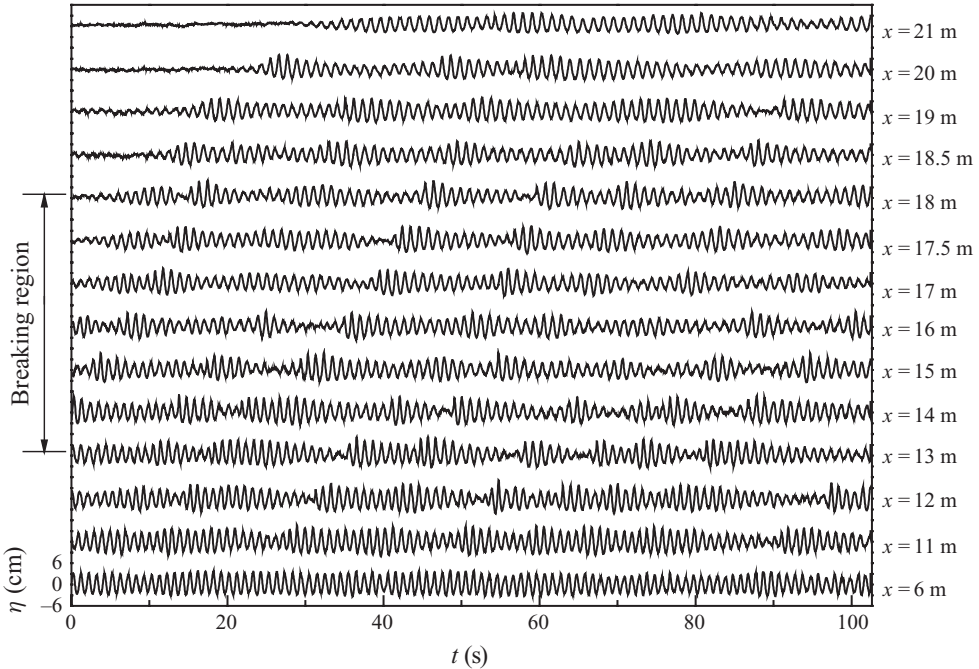
FIGURE 12. The measured surface elevations in the flume with an initial period 1.0 s and initial steepness 0.183 (Case 3). The breaking range was observed from $x = 13$ m to $x = 18$ m. As in figure 7, initial parts of the elevation measurements were recorded prior to arrival of the waves.

the phenomenon known as 'phase reversal' (Melville 1983), or 'phase jumps' (Huang *et al.* 1996). The physical mechanism of frequency downshift can be regarded as a continuous n to $n - 1$ wave fusion process (Huang *et al.* 1996). In this experiment, during the time span 20–102 s, the number of waves n, which was calculated via the zero-up-cross method, decreased from 80 at $x = 6$ m to 76 at $x = 18$ m, indicating that wave fusion occurred. If there is a 2π phase loss, two-to-one wave fusion occurs, causing an abrupt local frequency downshift (Huang *et al.* 1996). The largest local phase change in this experiment, case 1, was about 5 rad ($t = 62$ s at $x = 16$ m, and $t = 68$ s at $x = 17.5$ m; see figure 11), indicating that there was no two-to-one wave fusion or one-to-two wave fission. The above discussion suggests that the process of frequency downshift begins locally, but can be both abrupt and gradual.

4.3. *Modulation evolution of breaking waves*

In this section, modulation evolution of the waves for case 3, which had the largest initial steepness, is analysed. The breaking region of this experimental case ranged from $x = 13$ m to $x = 18$ m. The evolution of wave elevations is shown in figure 12. (Note that, due to the reflection limited time series, the recorded elevations are initiated prior to wavetrain arrival for some of the downwave locations.) Initially, the wave elevations are quite uniform, with only slight amplitude modulation. As waves evolved with distance, surface elevations underwent a modulation–demodulation–modulation process, i.e. wave modulation increased first, decreased slightly after wave breaking, and then increased again. The wave groups formed by the effects of instability had a steep front and a more gently sloping rear face. The instantaneous peak frequencies of those wave groups have a similar asymmetric form (as will be demonstrated later in this section). At the top of the bar the waves were not totally blocked, due to the
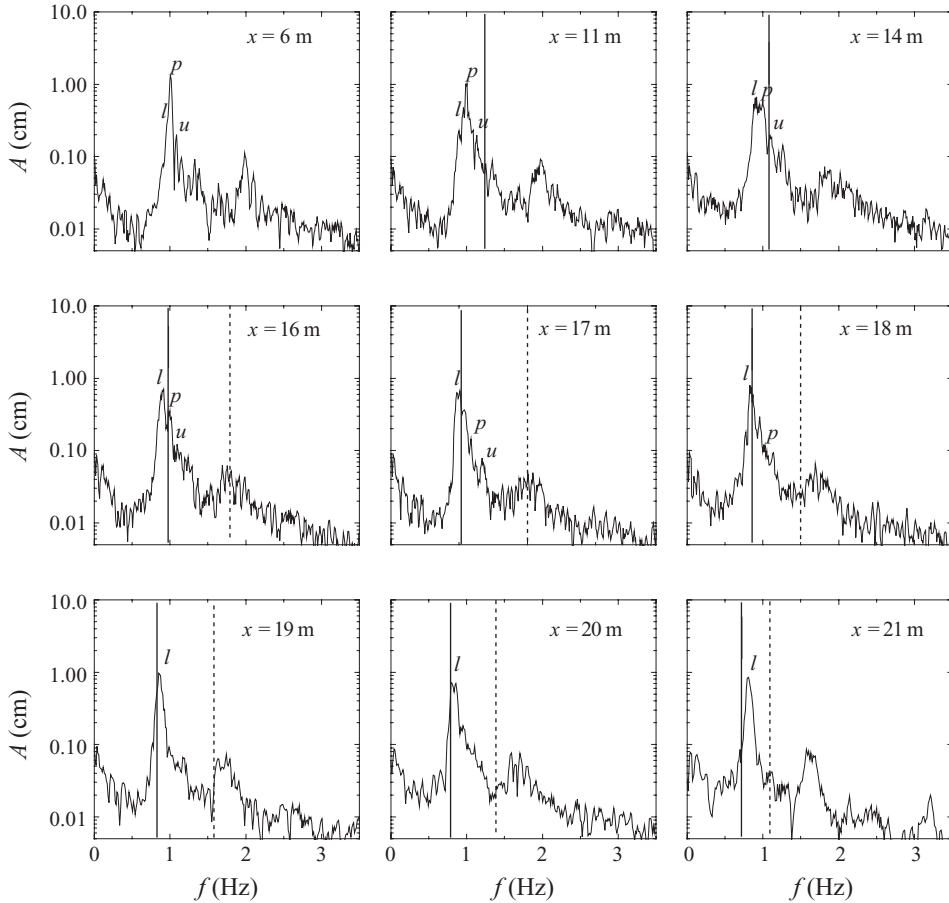
FIGURE 13. Evolution of spectra as a function of distance from the wavemaker for case 3 with initial $f_p = 1.0$ Hz ('l' denotes the lower sideband, 'p' indicates the initial peak waves, 'u' denotes the upper sideband). Each spectral estimate has 20 degrees of freedom and is within -23.5% to 44.6% of the 'true spectrum' at the 95% confidence level. The frequency resolution is 0.01 Hz for $x < 18$ m, and for $x = 18$, 19, 20 and 21 m, the frequency resolution is 0.0105, 0.012, 0.013 and 0.0142 Hz, respectively. Note that the breaking region of this case is from $x = 13$ m to $x = 18$ m. The vertical solid lines in each graph identify the local critical frequencies based on the linear dispersion relation. The vertical dashed solid lines in each graph identify the local critical frequencies based on the third-order Stokes dispersion relation.

relatively large frequency downshift (as will be discussed later). The amplitude spectra of surface elevations at select locations are shown in figure 13. The evolution of the wave spectra also indicates an instability involving a continuous frequency band rather than several distinct frequencies. The lower sideband energy grew with increasing distance, while the higher sideband energy exhibited little change. Eventually, the effective frequency downshift occurred following initial breaking ($x = 14$ m). In addition, figure 13 also shows that the blocking criterion predicted by the third-order Stokes dispersion relation is reasonable, indicating that amplitude dispersion has a significant effect. Based on the third-order Stokes dispersion relation, the primary waves for this case are not totally blocked, which is consistent with the experimental results.

The evolution of the instantaneous peak frequencies is shown in figure 14, and the mean values of the instantaneous peak frequencies for each measurement location are
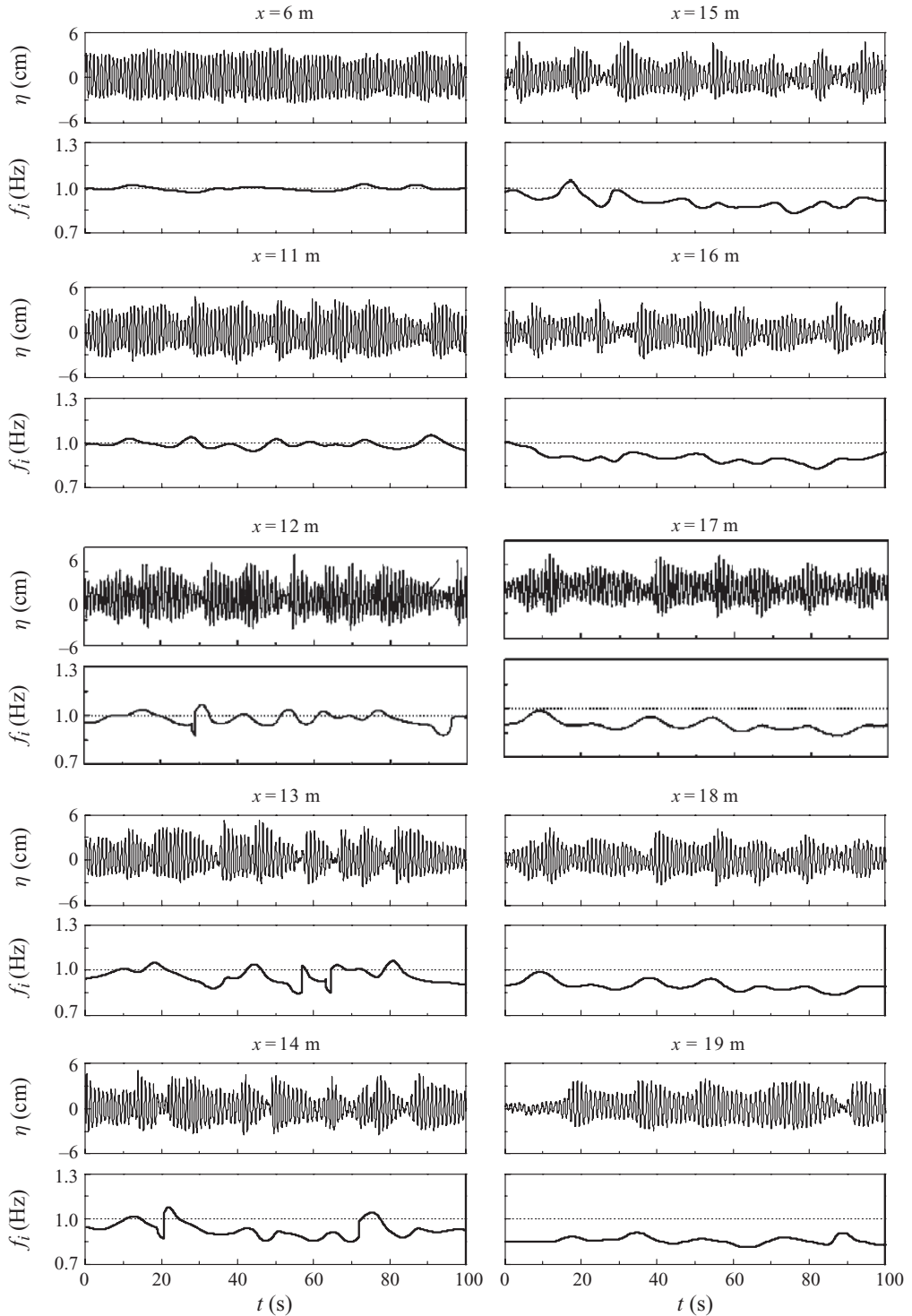
FIGURE 14. The evolution of the instantaneous peak frequency for case 3. This case has the largest initial steepness, as can be seen in table 1. The dotted line represents the initial peak wave frequency sent to the wavemaker. Instantaneous peak frequency was obtained by the Morlet-wavelet transform. The corresponding wave elevations are also shown for comparison.
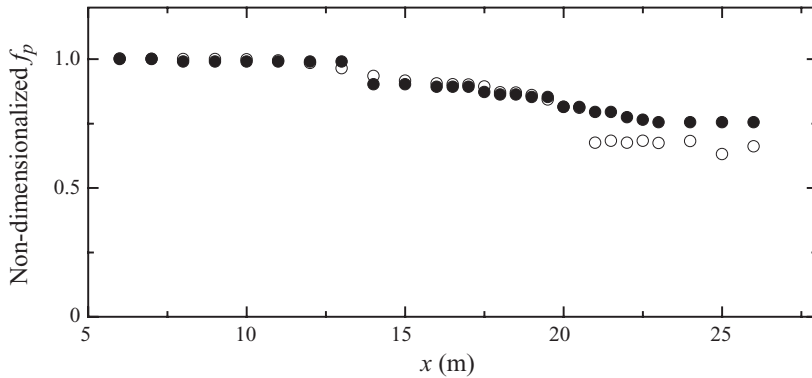
FIGURE 15. The mean values of instantaneous peak frequencies (open circles) for case 3, which were non-dimensionalized by the result measured at $x = 6$ m along the flume. The non-dimensionalized f_p (filled circles) obtained by FFT are also presented for comparison.

shown in figure 15. The mean values of instantaneous peak frequencies agree well with the results obtained by FFT. At the closest measurement location ($x = 6$ m), slight frequency modulation was observed. During some time spans, the local frequency is lower than the frequency, f_0, sent to the wavemaker, and for some time spans, the local frequency is higher than f_0. As distance increased, the frequency modulation increased with the amplitude modulation. Both local peak-frequency downshift and upshift were detected. At $x = 13$ m, the variations of instantaneous peak frequency over time are relatively large. Note that the frequency modulation of case 1 at this location is small (see figure 9), suggesting that wave modulation is closely related to the initial wave steepness, consistent with the results for quiescent water. As waves approached $x = 14$ m, the local peak frequency was usually lower than f_0, corresponding to an effective frequency downshift, as detected by the spectral analysis. The wave groups exhibited an asymmetric form with steeper forward faces and more gently sloping rear faces, caused by an asymmetric growth of sideband frequencies (Melville 1982). It is noted that abrupt changes in local peak frequency were smaller than those cases with smaller initial steepness. Moreover, no abrupt frequency jumps from a lower frequency to a higher frequency (much higher than f_0) were detected. This is very different from the non-breaking case presented. The primary reason for this phenomenon is that wave-breaking accelerated the process of the effective frequency downshift. As breaking occurred, waves at higher frequency lose energy, and also some energy was blocked by the opposing current, hence, the effective frequency downshift occurred more rapidly. Energetic waves with lower frequency are more stable than waves with higher frequency. As waves enter the region $x > 15$ m, no abrupt change of frequency was observed, and the wave peak frequency gradually reduced. The detrended phases of the measured elevations show that there were no phase jumps larger than 2π; see figure 16. The largest local abrupt phase jump of this experiment was approximately 4.4 rad, which occurred at about 57 s for $x = 13$ m (figure 16).

The number of waves, n, decreased from 101 at $x = 6$ m to 86 at $x = 18$ m, exhibiting a wave-fusion process. As the formed wave groups were more regular than the case with small initial steepness, it is easy to identify the wave-fusion process at adjacent locations. Figures 17 and 18, respectively, show the process of n to $n - 1$ wave fusion (also called 'crest pairing' by Ramamonjiarisoa & Mollo-Christensen 1979).
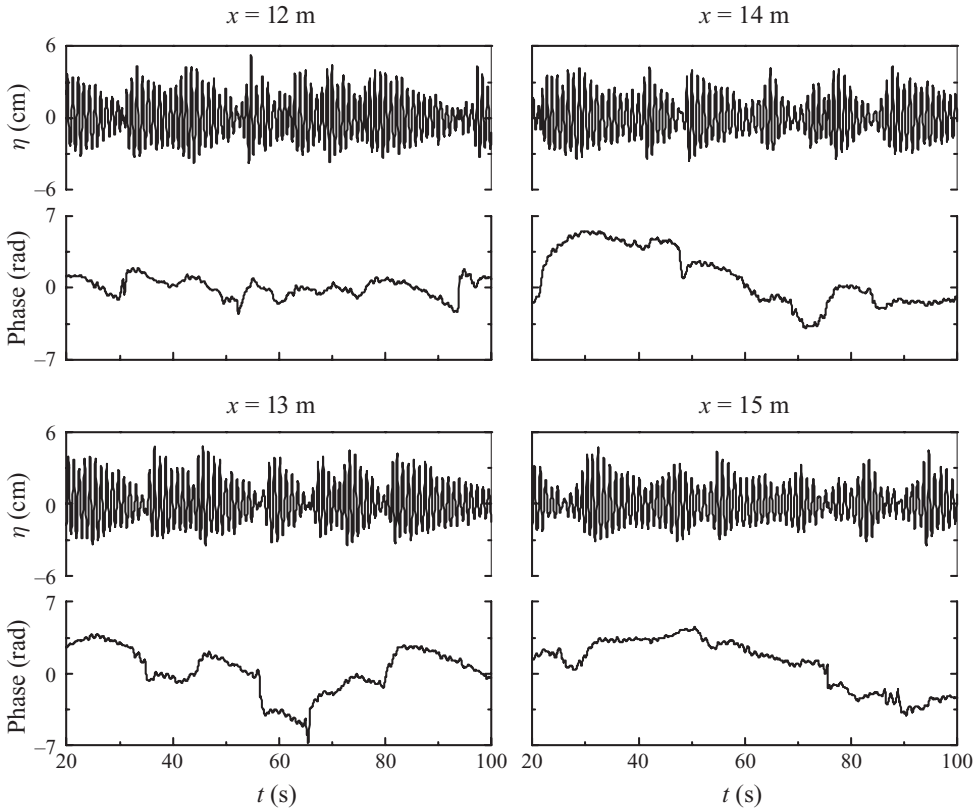
FIGURE 16. The detrended phase function of the surface elevations measured at four different locations for case 3.

The corresponding local frequency of the region of wave fusion is the smallest (see figure 14). From these wave records, it is also noted that the wave-fusion process tends to appear near a region of low wave energy, which is consistent with previous observations (Melville 1982; Huang *et al.* 1996; Tulin & Waseda 1999).

5. Concluding remarks

The evolution of wave modulation in a spatially varying opposing current was studied in a physical wave–current flume. Regular waves with different initial steepness ($0.05 < s < 0.19$) were considered, including non-breaking and breaking cases. Sideband frequencies arose ubiquitously from the background noise of the flume. As waves evolved, both amplitude and frequency modulations increased over short distances, suggesting that an opposing current can accelerate the evolution to instability. A peak-frequency downshift phenomenon was identified in both non-breaking and breaking experiments. Due to the presence of an opposing current, which can block the carrier waves, the peak-frequency downshift was observed even in waves with small initial steepness (smaller than 0.10), which is consistent with the results of Chawla & Kirby (2002). It must be mentioned that, in the present facility, wave modulation and peak-frequency downshift were not observed in experiments with larger steepness in both quiescent water and in the presence of a weaker opposing current. The ultimate peak-frequency downshift increased with an increase in the
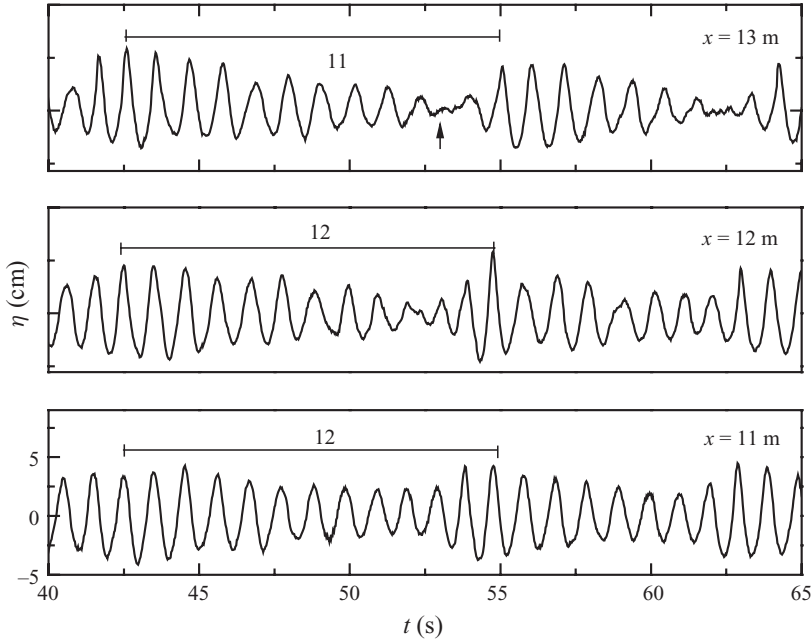
FIGURE 17. The decrease in the number of waves (12 waves being transformed into 11 waves) before the effective peak-frequency downshift occurred for case 3. The lower and upper panels are time-shifted. The arrow identifies when the number of waves decreased.
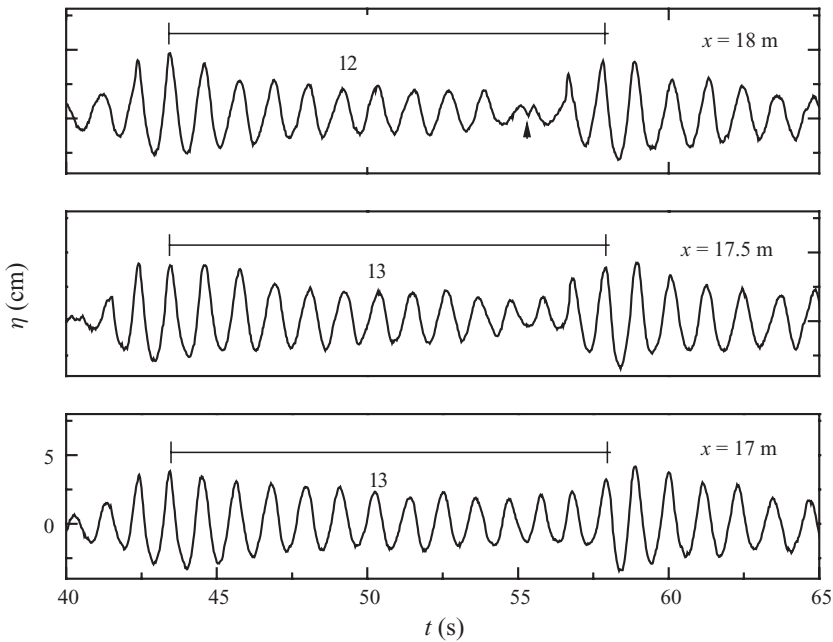

FIGURE 18. The decrease in the number of waves (13 waves being transformed into 12 waves) after the effective frequency downshift occurred for case 3. The lower and upper panels were time-shifted. The arrow identifies when the number of waves decreased.

initial steepness. The evolution of the spectrum of waves showed that the wavetrain is unstable to a band of frequencies rather than a few discrete frequencies, which is consistent with the results of Melville (1982), who conducted experiments without a spatially varying opposing current.

The frequency modulation of waves was observed through instantaneous peak frequency content extracted via the continuous wavelet transform. As waves evolved, the frequency modulated simultaneously with the amplitude. The near-uniform wavetrain gradually deteriorated into several wave groups with steeper forward faces and more gently sloping rear faces (due to the asymmetric modulation of frequency). The instantaneous frequency showed that the peak-frequency downshift begins locally, and gradually expands, indicating that the peak-frequency downshift is both local and gradual. However, abrupt changes of local frequency were also identified, suggesting that the peak-frequency downshift may also exhibit an abrupt character. The phase function also exhibited local abrupt changes, i.e. local abrupt jumps, corresponding to the phenomenon of phase reversal. The number of waves, n, decreased as waves propagated downwave, suggesting that the physical mechanism of frequency downshift in an opposing current may also be explained by wave fusion (Huang *et al.* 1996) or crest pairing (Ramamonjiarisoa & Mollo-Christensen 1979).

An opposing current not only increased the wave steepness and shortened the energy-transfer time, but it also destroyed the conservation of downwave–wave action, and then accelerated the process of frequency downshift. As wavetrains propagated in a spatially increasing opposing current, carrier-frequency waves and upper sideband waves and then higher harmonics are blocked gradually by the opposing current. For breaking waves, energy losses occurred at primary waves and some energy was blocked by the opposing current, so that the effective peak-frequency downshift occurred earlier than for non-breaking cases.

REFERENCES

BENJAMIN, T. B. & FEIR, J. E. 1967 The disintegration of wave trains on deep water. *J. Fluid Mech.* **27**, 417–430.

BRETHERT, F. P. & GARRETT, C. J. R. 1968 Wavetrains in inhomogeneous moving media. *Proc. R. Soc. Lond. Ser.* A *Math. Phys. Sci.* **302** (1471), 529–554.

CHAWLA, A. & KIRBY, J. T. 2002 Monochromatic and random wave breaking at blocking points. *J. Geophys. Res.* **107** (C7), 4-1-19.

CHERESKIN, T. K. & MOLLO-CHRISTENSEN, E. 1985 Modulational development of nonlinear gravity-wave groups. *J. Fluid Mech.* **151**, 337–365.

CHIANG, W. S. & HWUNG, H. H. 2007 Steepness effect on modulation instability of the nonlinear wave train. *Phys. Fluids* **19**, 1–13.

DELPRAT, N., ESCUDIÉ, B., GUILLEMAIN, P., KRONLAND-MARTINET, R., TCHAMITCHIAN, P. & TORRÉSANI, B. 1992 Asymptotic wavelet and Gabor analysis: extraction of instantaneous frequency. *IEEE Trans. Inf. Theory* **38** (2), 644–664.

VAN DUIN, C. A. 1999 The effect of non-uniformity of modulated wavepackets on the mechanism of Benjamin–Feir instability. *J. Fluid Mech.* **399**, 237–249.

FARGE, M. 1992 Wavelet transforms and their applications to turbulence. *Annu. Rev. Fluid Mech.* **24**, 395–457.

GERBER, M. 1987 The Benjamin–Feir instability of a deep-water Stokes wavepacket in the presence of a non-uniform medium. *J. Fluid Mech.* **176**, 311–332.

HARA, T. & MEI, C. C. 1991 Frequency downshift in narrowbanded surface waves under the influence of wind. *J. Fluid Mech.* **230**, 429–477.

HASSELMANN, K. 1962 On the non-linear energy transfer in a gravity-wave spectrum. Part 1. General theory. *J. Fluid Mech.* **12**, 481–500.

HUANG, N. E., LONG, S. R. & SHEN, Z. 1996 The mechanism for frequency downshift in nonlinear wave evolution. *Adv. Appl. Mech.* **32**, 59–117.

HUANG, N. E., LONG, S. R., TUNG, C. C., DONELAN, M. A., YUAN, Y. L. & LAI, R. J. 1992 The local properties of ocean surface-waves by the phase-time method. *Geophys. Res. Lett.* **19** (7), 685–688.

HWUNG, H. H., CHIANG, W. S. & HSIAO, S. C. 2007 Observations on the evolution of wave modulation. *Proc. R. Soc.* A *Math. Phys. Engng Sci.* **463** (2077), 85–112.

KIJEWSKI-CORREA, T. & KAREEM, A. 2006 Efficacy of Hilbert and wavelet transforms for time-frequency analysis. *J. Engng Mech.* **132** (10), 1037–1049.

LAI, R. J., LONG, S. R. & HUANG, N. E. 1989 Laboratory studies of wave-current interaction: kinematics of the strong interaction. *J. Geophys. Res. Oceans* **94** (C11), 16201–16214.

LAKE, B. M., YUEN, H. C., RUNGALDIER, H. & FERGUSON, W. E. 1977 Nonlinear deep-water waves: theory and experiment. Part 2. Evolution of a continuous wave train. *J. Fluid Mech.* **83**, 49–74.

LO, E. & MEI, C. C. 1985 A numerical study of water wave modulation based on a higher-order nonlinear Schrödinger equation. *J. Fluid Mech.* **150**, 395–416.

MALLAT, S. 1999 *A Wavelet Tour of Signal Processing*, p. 637. Academic Press.

MELVILLE, W. K. 1982 The instability and breaking of deep-water waves. *J. Fluid Mech.* **115**, 165–185.

MELVILLE, W. K. 1983 Wave modulation and breakdown. *J. Fluid Mech.* **128**, 489–506.

PHILLIPS, O. M. 1960 On the dynamics of unsteady gravity waves of finite amplitude. Part 1. The elementary interactions. *J. Fluid Mech.* **9**, 193–217.

RAMAMONJIARISOA, A. & MOLLO-CHRISTENSEN, E. 1979 Modulation characteristics of sea-surface waves. *J. Geophys. Res. Oceans Atmos.* **84** (NC12), 7769–7775.

SU, M. Y. 1982 Evolution of groups of gravity waves with moderate to high steepness. *Phys. Fluids* **25** (12), 2167–2174.

TORRENCE, C. & COMPO, G. P. 1998 A practical guide to wavelet transform. *Bull. Amer. Meteorol. Soc.* **78** (1), 61–78.

TULIN, M. P. & WASEDA, T. 1999 Laboratory observations of wave group evolution, including breaking effects. *J. Fluid Mech.* **378**, 197–232.

TURPIN, F., BENMOUSSA, C. & MEI, C. C. 1983 Effects of slowly varying depth and current on the evolution of a Stokes wavepacket. *J. Fluid Mech.* **132**, 1–23.

WASEDA, T. & TULIN, M. P. 1999 Experimental study of the stability of deep-water wave trains including wind effects. *J. Fluid Mech.* **401**, 55–84.